ORIGINAL ARTICLE

IJAMB JOURNALAMB.COM
INTERNATIONAL JOURNAL OF ADVANCES IN MEDICAL BIOTECHNOLOGY

Photoluminescent gels based on han purple: new frontiers in biotechnology

K.F. Santos[1,2]; C.Y. Morassutia[1*]*; D.A. Ribeiro[2]; K.V.S. Carvalho[1]; M.A. Sabino[1,2]; J.V.L Silva[1]; J.K.M.B. Daguano[1,3]

*Corresponding author: E-mail address: claudio.morassuti@cti.gov.br

Received: October 2024; Accepted: December 2024.

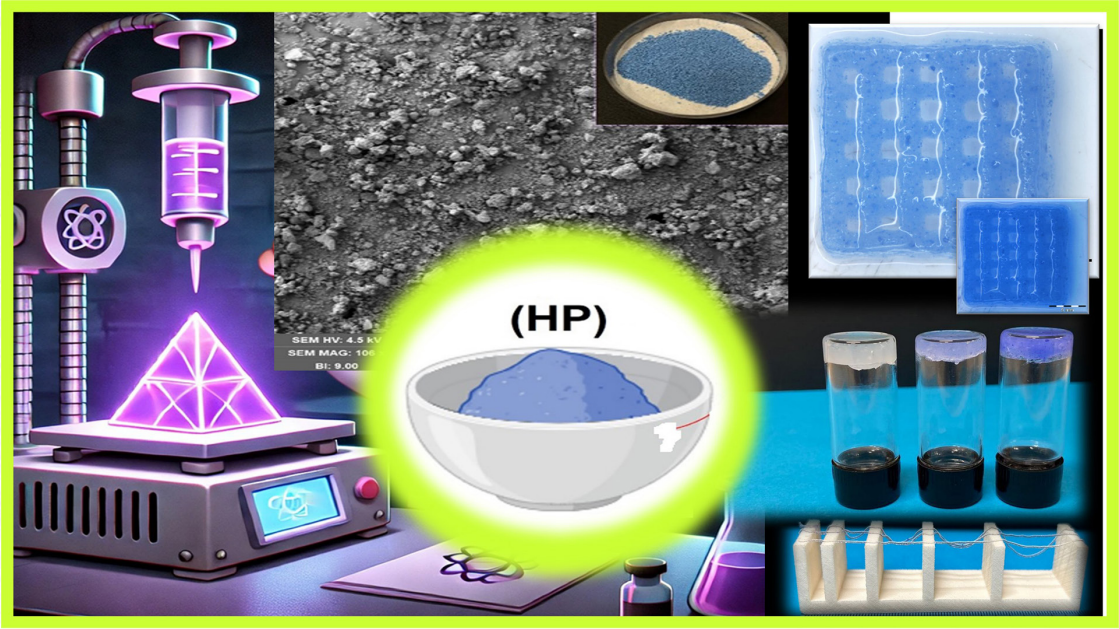

Abstract: As a result of the increasing need for new biocompatible materials, polymer-based gels have become promising options. Lately, photoluminescent gels have shown potential for applications in biotechnology and non-invasive tracking due to their ability to emit light when temperature changes occur. This research investigates the incorporation of Han Purple (HP) pigment into a polyethylene glycol/Laponite matrix [92,5/7,5%] (P7LHP0%) to produce a 3D-printed gel. The gels were examined for possible use as smart sensors, focusing on their optical and thermal characteristics. Formulations with HP concentrations of 0.0%, 0.5%, and 2.0% were prepared, followed by extrusion-based 3D printing. Characterization techniques included FTIR, SEM, and optical analyses (emission and excitation spectra). The findings showed 3D structures with good shape fidelity while FTIR indicated suitable compatibility between HP and the matrix. Optical analysis revealed fluorescence with an excitation band between 400 and 700 nm, with a maximum at 620 nm, and an emission band at 830 - 1000 nm with a peak at 925 nm. This study highlights the potential of HP as a promising material for fluorescent gels in 3D printing, creating new opportunities for biotechnology applications.

Keywords: Han Purple. Fluorescence. Responsive gels. Optical sensors. 3D printing. Biotechnology.

[1]Renato Archer Information Technology Center, Campinas, SP, Brazil.
[2] Chemistry Department, Research Group B5IDA, Simon Bolivar University, 8900, Caracas, Venezuela
[3]Federal University of ABC (UFABC), Center for Engineering, Modeling and Applied Social Sciences (CECS), São Bernardo do Campo, SP, Brazil.

https://doi.org/e10.52466/ijamb.v6i2.129

"A Tribute to Dr. Jorge Vicente Lopes da Silva"

Introduction

The search for materials with innovative properties is crucial for the progress of science and technology, especially in areas such as biotechnology, biomedicine, and pharmacology [1]. Han Purple (HP), a pigment with both historical significance and promising functional characteristics, has recently sparked interest. Originally developed in ancient China around 700 BCE, HP exhibits a purple color and was widely used in embellishing various artifacts, including vases, bricks, and walls. However, beyond its artistic value, the physical and chemical characteristics of HP make it an appealing candidate for modern technological applications[2].

The chemical formula of HP is predominantly $BaCuSi_2O_6$, and it stands out not only for its relatively straightforward synthesis but also for its fluorescent properties, attributed to the presence of Cu^{2+} ions within its structure[2]. The synthesis process involves the combination of precursors such as barium carbonate ($BaCO_3$), silicon dioxide (SiO_2), and copper oxide (CuO) under precise thermal control[3,4]. These unique characteristics allow HP to emit fluorescence within the near-infrared spectrum (NIR), unlocking new possibilities for its application in biomedical sensors, fluorescent markers, and infrared imaging techniques [2,5].

In parallel, hydrogel-based biomaterials have become essential in tissue engineering due to their ability to absorb large volumes of water and simulate the conditions of the cellular environment. The development of three-dimensional scaffolds using additive manufacturing techniques, such as 3D printing, has facilitated the reproduction of complex structures that mimic the behavior of natural tissues.

Polyethylene glycol (PEG) stands out as a prominent polymer in this area due to its biocompatibility and versatility. Nevertheless, PEG by itself does not possess the necessary rheological properties to satisfy the requirements of 3D printing, limiting its direct applicability[6]. To overcome these limitations, rheological modifiers like Laponite XLG—a nanosilicate—are incorporated into the PEG matrix, forming a three-dimensional network that maintains structural integrity during the printing process [7,8]. This PEG/Laponite combination results in rheologically stable gels, ideal for fabricating complex structures suitable for a wide range of biomedical applications[9].

The current study aims to synthesize and characterize HP and incorporate it into gels based on a PEG/Laponite matrix, to create a NIR fluorescence and printable gel and explore the HP emissions in response to temperature variations[9,10]. By integrating this purpure pigment into hydrogels, this research not only seeks to expand the understanding of fluorescent material functionalization but also aims to open new opportunities for its application in biotechnology and regenerative medicine.

Experimental

Materials

This study utilized Polyethylene glycol-400 (PEG) with a molecular weight range of 380–420 $g.mol^{-1}$ (Dinâmica) and Laponite XLG (Colormix). The reagents for the synthesis of Han Purple (HP) included barium carbonate ($BaCO_3$), silicon dioxide (SiO_2), and copper oxide (CuO), all sourced from Dinâmica.

Synthesis of HP

The HP pigment was produced by combining barium carbonate ($BaCO_3$), silicon dioxide (SiO_2), and copper oxide (CuO) in a 1:2:1 molar ratio, following the procedure described by McDaniel et al. (2014)[4]. The components were homogenized using a high-speed mixer (SpeedMixer™ - Hauschild DAC 250), at 1100 rpm for 5 minutes. After homogenization, the carbonate-silica-oxide mixture was subjected to thermal sintering cycles. At first, the mixture was heated to 1000°C at a heating rate of 7°C/min. Following this step, the powder was deagglomerated and exposed to a second thermal cycle at 1050°C with a heating rate of 5°C/min. After high-temperature processing, the material gradually cooled to room temperature (25°C) [4]. The overall equation (Eq. 1) describing the chemical reaction involves the decomposition of $BaCO_3$ and the subsequent formation of the fluorescent $BaCuSi_2O_6$ phase of HP:

$$BaCO_{3(s)} + 2SiO_{2(s)} + CuO_{(s)} \rightarrow BaCuSi_2O_{6(s)} + CO_{2(g)} \quad (1)$$

X-ray Diffraction (XRD)

X-ray diffraction measurements were performed using a Rigaku Miniflex 600. The X-ray source was set to 40 kV and 15 mA, employing the Kα (Cu) line. The setup included a Soller slit (inc) of 5.0°, IHS of 5.0 mm, SS of 1.250°, DS of 1.250°, and RS of 0.3 mm. Data acquisition was carried out at a scanning rate of 1.5°/min with a step size of 0.02°.

Scanning Electron Microscopy (SEM)

The synthesized HP powder was characterized using scanning electron microscopy (SEM) with a FEG-MIRA 3 (TESCAN) instrument to assess its superficial morphology. The samples were coated with a 10 nm gold-layer to ensure conductivity and were analyzed at a voltage of 4.5 kV.

Optical Characterizations

Optical Absorption

Optical absorption was measured at room temperature using a Perkin Elmer Lambda 1050

spectrophotometer. The spectra were recorded over the range of 300 to 1500 nm. Diffuse reflectance measurements of powder samples were conducted using a 150 mm integrating sphere accessory.

Temperature-Dependent Emission Spectra

Emission spectra as a function of temperature were collected using an Ocean Optics Maya Pro 2000 spectrometer connected via an optical fiber. Measurements were conducted over the range of 200 to 1100 nm. The samples were excited by a rhodamine 6G dye laser at 612.76 nm with a power output of 2.0 ± 0.2 mW. To eliminate excitation interference, a 650 nm long-pass filter was used during emission data collection. The sample temperature was controlled between 293 K and 343 K using a REX C100 controller and a type-K thermocouple.

Excitation-Emission Mapping

Excitation-emission maps were generated using a Horiba Instruments Duetta spectrometer. To acquire the emission spectra, excitation wavelengths ranging from 400 to 700 nm with an increment of 5 nm were used. The integration time for emission signal acquisition was 4 seconds and excitation and emission slit widths were both set at 5 nm. Emission spectra were recorded from 715 nm to 1000 nm, with a 715 nm long-pass filter placed at the emission collection port to exclude excitation line interference.

Chemical Composition Analysis

The chemical composition of the gels was evaluated using a Perkin Elmer Spectrum 100 in attenuated total reflection (ATR) mode. Spectra were acquired over the range of 450 to 4500 cm^{-1} with a resolution of 4 cm^{-1}, and each spectrum is an average of 16 consecutive acquisitions of the same sample.

VIS/NIR Microscopy

A HiView digital microscope was employed for optical imaging. The built-in microscope illumination was used to acquire visible images. For red excitation imaging, a 620 nm LED source (50.0 ± 0.5 mW) was applied. In near-infrared (NIR) imaging, only the 620 nm excitation was maintained, with a 715 nm long-pass filter placed at the microscope port to ensure that only the emission radiation from HP contributed to NIR image formation.

Preparation of HP-doped gels

The preparation of PEG-Laponite gels with 7.5 wt% nanosilicate (referred to as $P7L^{HPO\%}$) followed the method described by Santos et al. (2022) [7]. Initially, a 44 vol% PEG solution was mixed with Laponite using the SpeedMixer™ at a speed of 1000-1200 rpm for 2 minutes[7]. The resulting gel was stored at 4-8°C for 48 hours for the aging process.

After preparing the base $P7L^{HPO\%}$ gel, Han Purple (HP) was incorporated at concentrations of 0%, 0.5%, and 2% (w/w), resulting in the formulations named $P7L^{HPO\%}$ $P7L^{HPO.5\%}$, and $P7L^{HP2\%}$ respectively, based on the total gel mass.

To ensure optimal dispersion of HP particles, the gels were further homogenized in the SpeedMixer™ at 1000-1200 rpm for an additional 2-5 minutes. This ensured the thorough integration of HP into the $P7L^{HPO\%}$ gel matrix. Figure 1 illustrates the entire process, from the synthesis of the pigment to its application in PEG-Laponite-based gels.

Qualitative Analysis of the Gels Before 3D Printing

Subsequently, the gels were kept refrigerated (6.0 ± 2.0 °C) until the 3D printing stage. Before printing tests, discs (2.5 ± 0.1 mm in height and 9.5± 0.1 mm in diameter) were prepared and examined under an Olympus SZX16 stereomicroscope to verify the homogeneous dispersion of HP in the $P7L^{HPO\%}$ matrix.

Although the properties of the $P7L^{HPO\%}$ gels have been reported in previous studies, the addition of HP required a new qualitative analysis to assess potential changes in rheological properties, particularly those related to 3D printing. A platform model with known distances, ranging from (0.5, 1.5, 2.0, and 2.5) cm, was used to evaluate the collapse of filaments. Additionally, the sol-gel transition over time was observed through the inversion test.

Printing of Scaffold

The *BioScaffold v. 2.0* software was used to generate printing data for scaffolds with dimensions of 10 mm × 10 mm × 2 mm, consisting of 10 layers. The printing speed was set to 12 mm/s, and a 410 µm diameter nozzle (20G) was employed. The scaffolds were printed using a 593iCAN printer, equipped with a dual extrusion head system[11]. The whole process was carried out at room temperature (25°C). After printing, the scaffolds were photographed with a stereomicroscope.

The printability (Pr) index was calculated to assess the shape fidelity of the printed scaffolds. This helps evaluate how accurately the produced structures align with the intended design. The calculation follows Eq. 2 [12,13].

$$Pr = \frac{L^2}{16A} \quad (2)$$

Where: (A) is the pore area, (L) is the pore perimeter, and (Pr) is the printability index.

Results and Discussion

Analysis of Synthesized HP Powder

Figure 1 presents the micrograph of the HP powder following synthesis. Figure 2(a) confirms that the HP powder was successfully obtained, exhibiting the expected purple coloration, a characteristic attributed to the presence of barium carbonate in its composition[14]. The analysis of Figures 2(b) and 2(c) reveals that the particle distribution in the sample was less homogeneous than anticipated for this pigment. The images highlight that the HP particles display irregular shapes, and many aggregates were observed due to the absence of conventional treatment steps[3]. Furthermore, the thermal treatments applied resulted in larger particle sizes, indicating that high temperatures promoted stronger bonding between the particles, resulting in a more elongated shape[3,4].

In Figure 3, the synthesized HP powder exhibits purple coloration. The X-ray diffraction (XRD) pattern confirms the presence of the fluorescent phase associated with HP, with the molecular formula $BaCuSi_2O_6$. This phase exhibits fluorescence emission when excited in the red/NIR region [3,4]. Both the excitation and emission bands fall within the first transparency window of biological tissues, which enhances the potential of HP for non-invasive biomedical imaging applications[13].

From the synthesis of HP, it is difficult to predict the size of the formed inorganic particles, but it can be noted from the observations made by SEM that the distribution and morphological characteristics of the photoluminescent pigment have been verified and match the expected proportions. Can be observed in Figure 2(c) is that HP particles appear as agglomerates, which may obscure some phases that are by products of the synthesis, in this sense SEM micrographs only can show the orientation of the particles, while the XRD provides information about the preferred orientation of the crystals of this material. In the XRD diffractogram, there is no evidence indicating an additional phase or an alteration in the crystal structure; only the characteristic bands of HP are present in Figure 3.

Figure 4 presents the absorbance spectrum of the sintered HP powder over the range of 430 to 1200 nm. Two main absorption peaks are observed in the UV-VIS-NIR region: one at 580 nm (a) and the other at 765 nm (b), with the maximum absorption occurring at 580 nm. These absorption bands correspond to the $^2B_{1g} \rightarrow {}^2E_g$ and $^2B_{1g} \rightarrow {}^2B_{2g}$ transitions of Cu^{2+} ions present in the crystalline structure of the $BaCuSi_2O_6$ phase[1, 2, 14]. Therefore, laser excitation of the sample can be effectively performed using wavelengths near the maximum absorption, such as at 612.76 nm.

The emission spectra of HP at different temperatures, from 293 to 343 K, are shown in Figure 5, covering wavelengths from 750 to 1100 nm. Under excitation at 612.76 nm, an emission band in the near-infrared (NIR) region of 800 to 1100 nm ($^2B_{2g} \rightarrow {}^2B_{1g}$ transition) is detected. As the temperature increases, a suppression of fluorescence occurs due to the rise in the non-radiative decay rate of the $^2B_{2g}$ emitting level. It is crucial to mention that the presence of two convoluted emission bands in the emission profile is due to the spectrometer's spectral response [15]. This phenomenon is valuable for developing intensity ratio-based fluorescent temperature sensors. Figure 6 illustrates the ratio of emission areas at 893 nm and 985 nm, which is useful for precise temperature monitoring.

The intensity ratio (I_{893}/I_{985}) decreases nearly linearly as temperature increases. This behavior demonstrates that the system has the potential to be used as an optical temperature sensor with the Fluorescence Intensity Ratio (FIR) technique. To evaluate the sensor's sensitivity, the data were fitted according to the FIR theory [16,17], which Δ represents the intensity ratio. The theoretical framework is described in Eq. 3.

$$\Delta = \frac{I_{2j}}{I_{1j}} = \frac{g_2 \sigma_{2j} \omega_{2j}}{g_1 \sigma_{1j} \omega_{1j}} e^{\left[\frac{-\Delta E}{k_b T}\right]} = B\, e^{\left[\frac{-\Delta E}{k_b T}\right]} \quad (3)$$

In FIR theory, I_j and I_j represent the emission intensities of two energy levels of the ion of interest, g_{ij} is the degeneracy of the emitting level, σ_{ij} is the emission cross-section, and ω_{ij} is the angular frequency of the fluorescence transition from the higher level (i=2) to the lower level (i=1). Additionally, ΔE represents the energy difference between the thermally coupled levels, and k_B is the Boltzmann constant. For thermometric applications, it is crucial to calculate the sensitivity parameter of the technique for the levels being utilized. This sensitivity reflects how the fluorescence intensity ratio responds to changes in temperature Eq. 4 presents the relative sensitivity parameter (S_r)[18]:

$$S_r = \frac{1}{\Delta} \frac{d\Delta}{dT} = \left[\frac{\Delta E}{k_b T^2}\right] 100 \quad (4)$$

The absolute sensitivity is calculated as the first-order derivative of with respect to temperature. However, to enable the comparison between different materials, the relative sensitivity (Eq. 4) is presented. In this case, S_r is the derivative of Eq. 3, which is normalized by the function Δ itself and multiplied by 100 to express the values in [%/K] units. Figure 7 shows the relative sensitivity calculated from the data presented in Figure 5 for the same temperature range.

In Figure 7, it can be observed that sensitivity

decreases with increasing temperature, which is expected for FIR thermometers. The maximum sensitivity at 293 K was 0.3%/K. Although this sensitivity is considered low in the literature[19,20], it should be noted that both the excitation and emission wavelengths fall within the first transparency window of biological tissues[21], making it particularly attractive for biomedical applications. Another aspect of potential investigation in future research is the addition of impurities to enhance the fluorescence quenching effect. These impurities would aim to increase the phonon energy, further improving the material's performance.

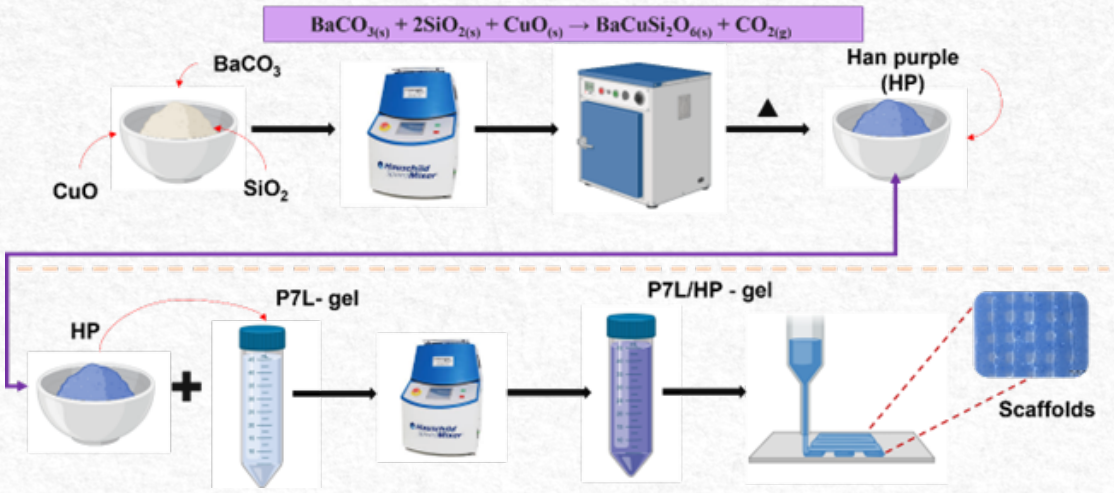

Figure 1 - Illustration of the pigment synthesis process, gel preparation, and sample printing. The images were created using the BioRender® visual tool. Source: Santos et al.

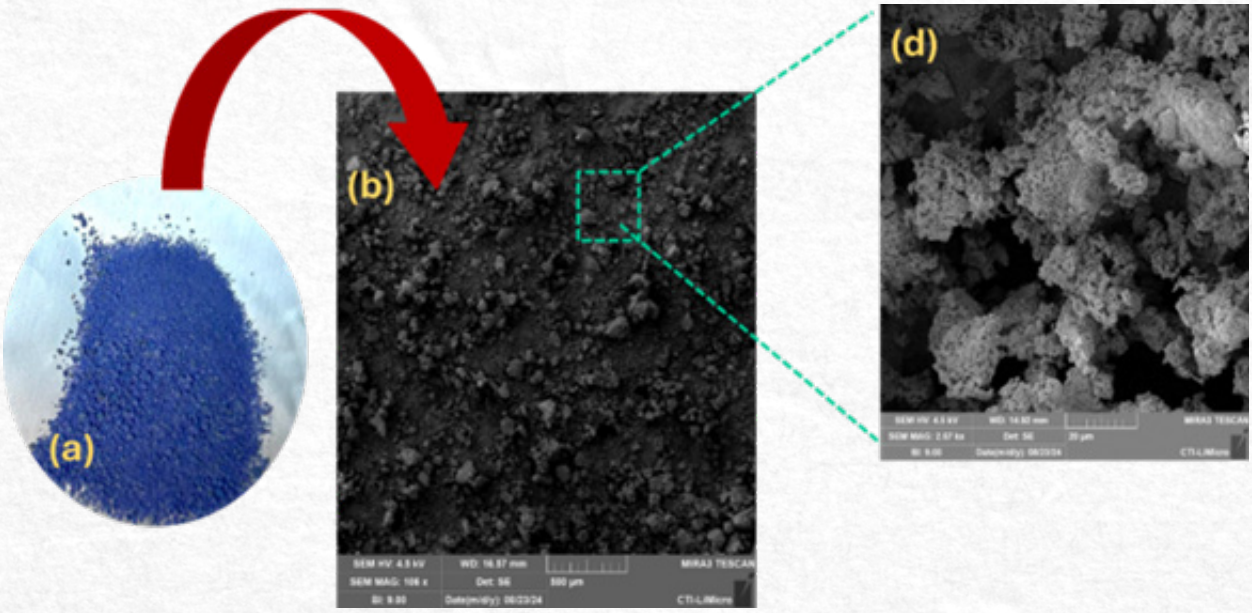

Figure 2 - Micrograph of HP powder after synthesis and morphology of its particles. Where (a) post-sintering powders and (b and c) correspond to powder morphology. Source: Santos et al.

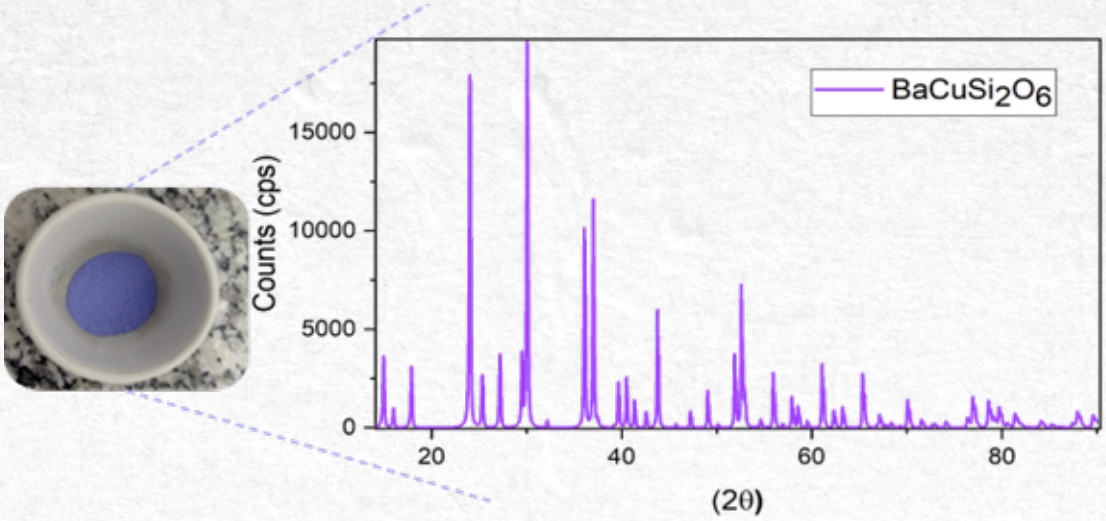

Figure 3 - Diffractogram of the synthesized sample; peaks are characteristics of HP pigment. Source: Santos et al.

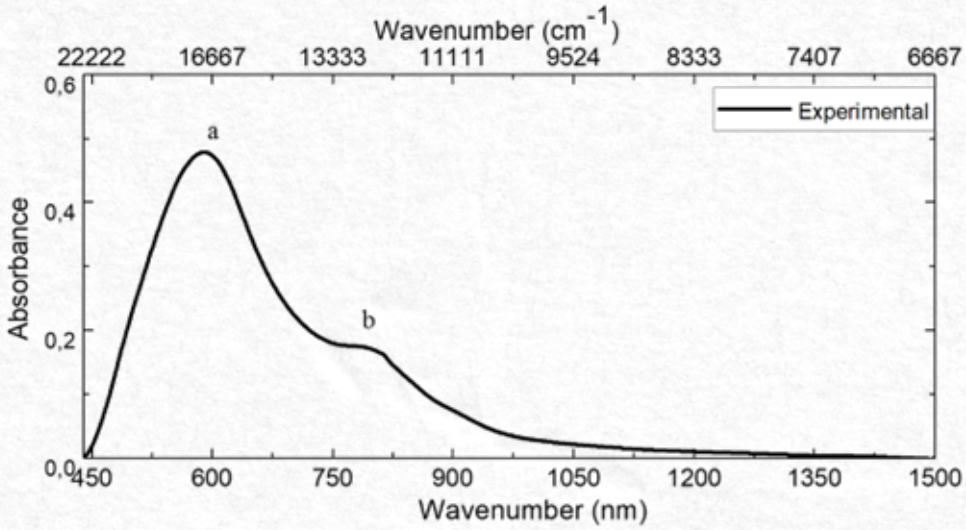

Figure 4 - Absorbance spectrum in the UV-VIS-NIR region for the synthesized HP sample. Source: Santos et al.

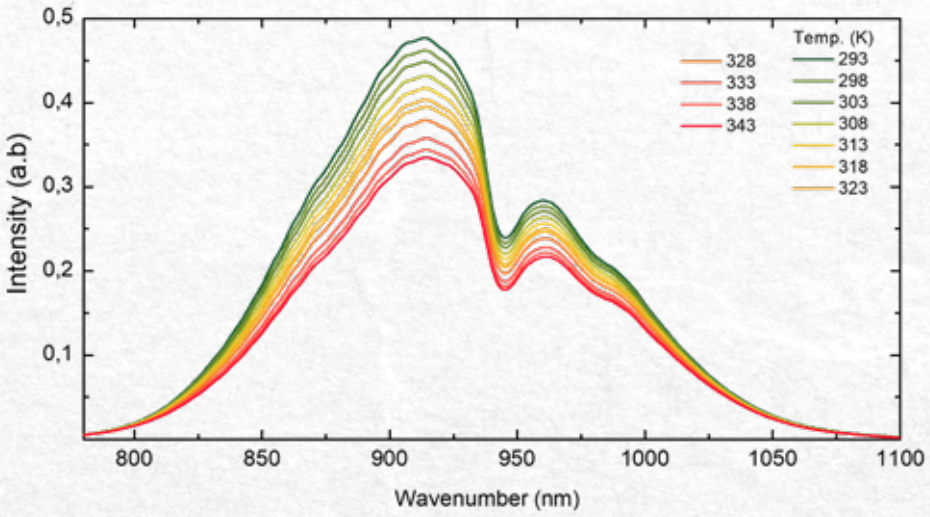

Figure 5 - HP emission at different temperatures, in the range of 293 to 343 K. Source: Santos et al.

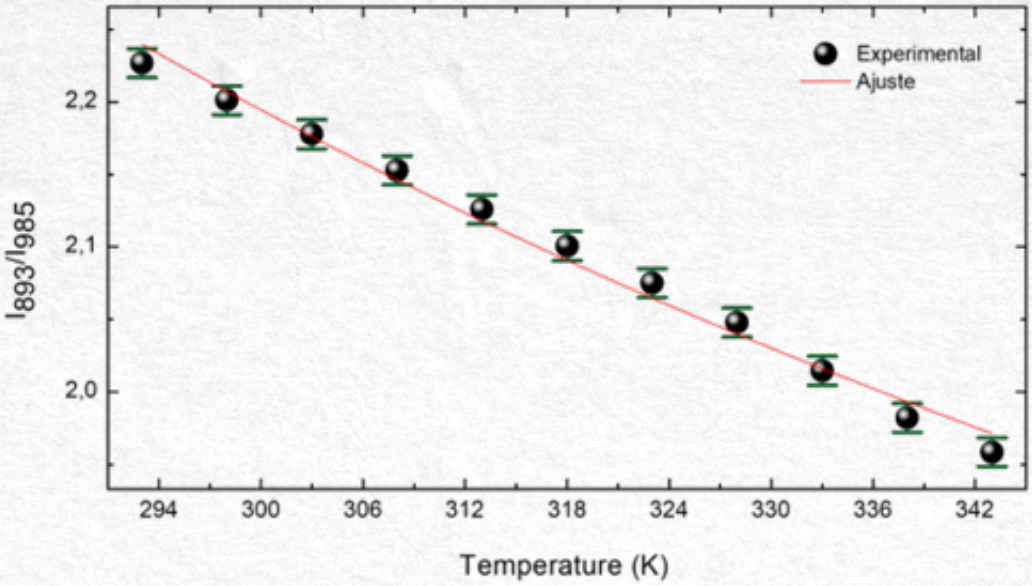

Figure 6 - Intensity ratio for emissions centered at 893 and 985 nm (I_{893}/I_{985}). Source: Santos et al.

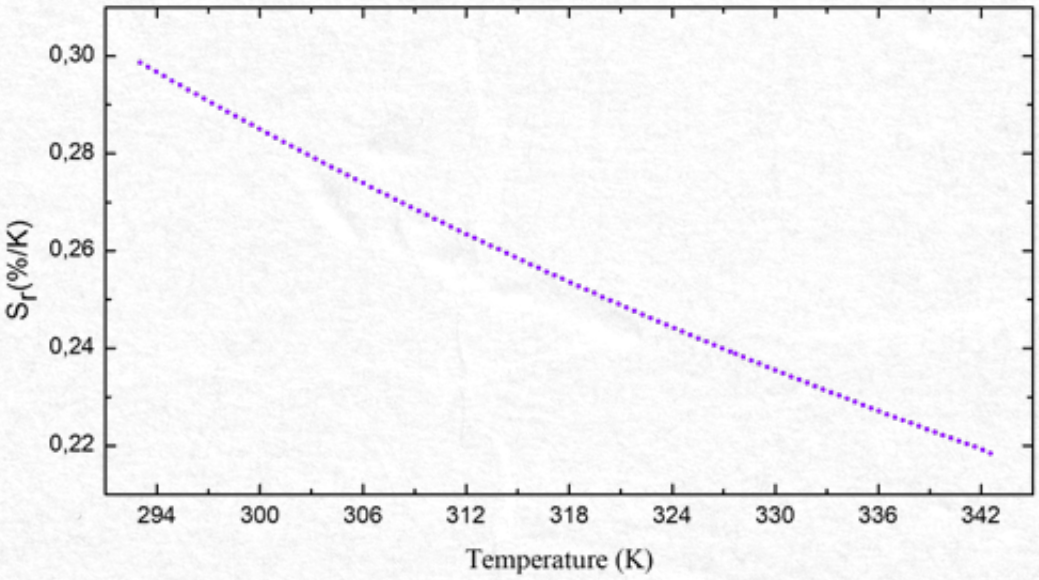

Figure 7 - Relative sensitivity (Sr) in the range of 293 to 343 K. Source: Santos et al.

Analysis of HP-Doped Gels

To investigate the compositional details of the gels produced with and without the incorporation of the HP pigment, the compositions were analyzed using Fourier Transform Infrared Spectroscopy (FTIR), as shown in Figure 8. It is observed that all the curves in Figure 8 exhibit similarities, with slight differences compared to the precursor gel P7L$^{HP0\%}$. The peaks corresponding to the P7L$^{HP0\%}$ formulation was previously described by Daguano et al. (2022)[7]. The bands in the 3677–3012 cm^{-1} region in the P7L$^{HP0,5\%}$ and P7$^{HP2\%}$ compositions are linked to the O-H stretching, which comes from the PEG precursor solution. The peaks at 2963 cm^{-1} and 2870 cm^{-1} correspond to the C-H methylene stretching from the PEG precursor. Additionally, the peaks at 1532 cm^{-1}, 1463 cm^{-1}, and 1246 cm^{-1}are associated with C-H stretching from methyl groups[22].

The peaks at 994 and 980 cm^{-1} can be attributed to the Si-O and Si-O-C bonds, respectively, due to the adsorption of the nanosilicate Laponite and silica present in HP, also detectable in the gel base [7,9]. The characteristic HP peaks ($BaCuSi_2O_6$), observed at 800 and 1100 cm^{-1}, are associated with Si-O antisymmetric stretching. It is suggested that the peaks in the 670 cm^{-1} region correspond to the Cu-O group, although they may be overlapping due to the presence of Laponite nanosilicates and HP silica. Finally, the formation of new peaks in the regions of 1645 and 845 cm^{-1} is observed in the compositions P7L$^{HP0,5\%}$ and P7L$^{HP2\%}$. The peak at 845 cm^{-1} can be attributed to the Cu-O group[2]. The peak at 1645 cm^{-1} is related to the vibrations of the carbonyl group C=O which may be produced in the PEG polymer chain through oxidation, a structural change possibly induced by HP presence. When the PEG gel is mixed with the inorganic HP and, if the photoluminescent compound could act as a photoactivator (generating free radicals) when exposed to UV/Vis light, these radicals can attack the PEG bonds and cause its photo-oxidation, generating carbonyl groups, as evidenced in the FTIR spectrum (peak at 1645 cm^{-1}) of the gels doped with HP[23]. This phenomenon appears to be independent of the HP concentration within the gel, relying instead on the mere presence of the photoluminescent compound. As Illustrated in Figure 10(c), the photoactivation of HP particles by visible light suggests that this process is more likely to occur in environments where the preparation or use of these gels involves oxygen and intense light exposure, or during their storage.

To assess the dispersion of HP particles, discs

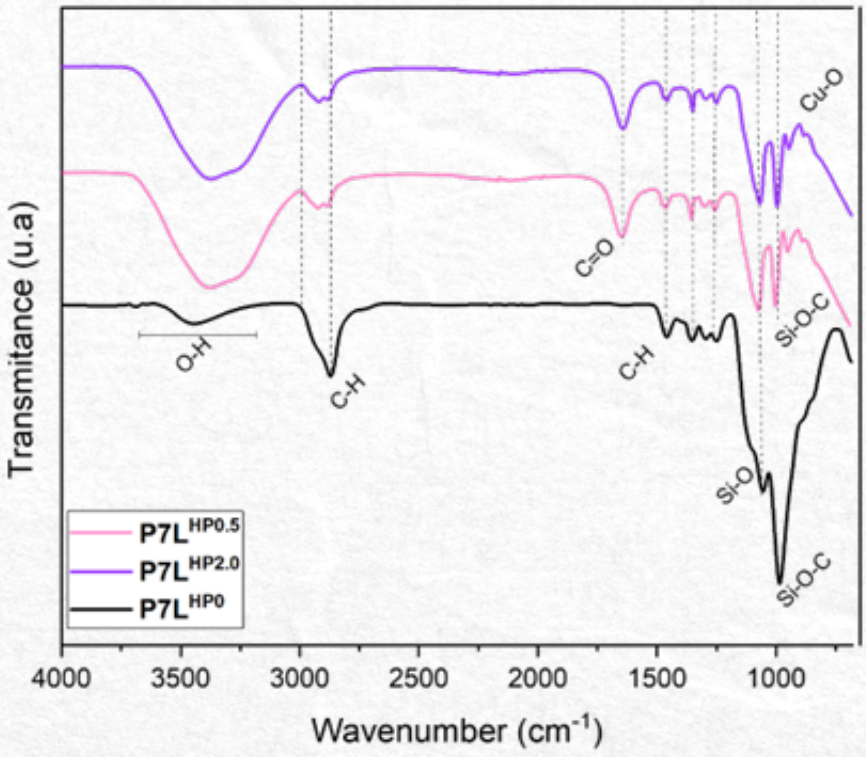

Figure 8 - FTIR analysis of P7LHP0.5% and P7LHP2% gels with HP content of 0.5 and 2% respectively. The P7LHP0% gel was used as a control due to the absence of pigments. Source: Santos et al.

with a 10 mm-diameter were produced, as illustrated in Figure 9. The addition of HP resulted in a color shift toward a bluish hue, with pigmentation intensity increasing proportionally to the HP concentration. Particle dispersion was considered satisfactory in all formulations; however, the P7L$^{HP2\%}$ sample exhibited a more homogeneous distribution of particles. In the 0.5% HP formulation, some noticeable particle agglomerations were observed, more prominent than in the 2% HP discs.

Preliminary qualitative tests were carried out to assess the suitability of the photoluminescent gels for printing, as shown in Figure 10. In Figure 10(a), the gel-filled tubes were kept upside down for 24 hours without any movement observed, indicating sufficient stability for the printing process. Previous studies by Santos and Daguano provided a detailed description of the rheological properties of the base gel PEG/Laponite (PL), offering a solid understanding of the rheological properties of this gel [7,9]. In the case of gel formulations with HP, given their low percentage, it is possible that this does not generate substantial changes in its rheological behavior. These tests also contributed to a better understanding of the gelation process, confirming promising characteristics for printing[24,25]

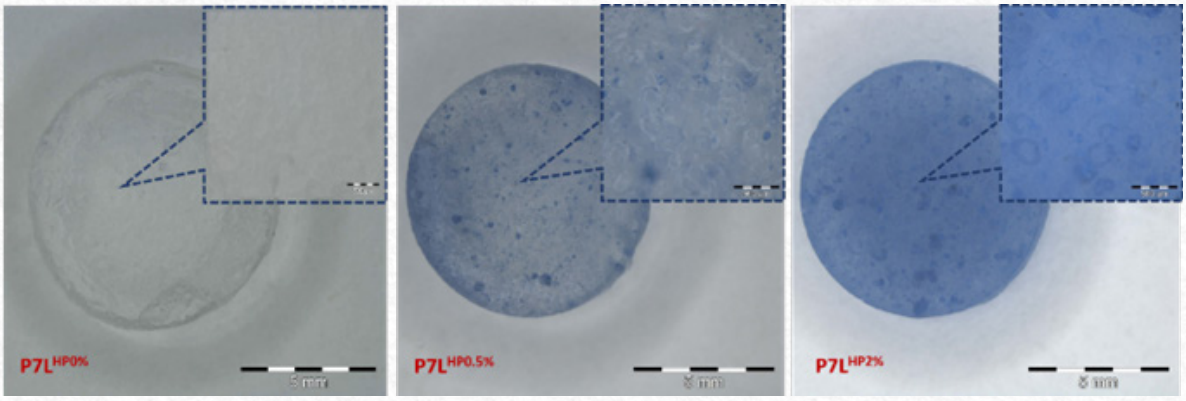

Figure 9 - Tablets made from gels formulated with doping concentrations of: 0%, 0.5%, and 2% HP. Source: Santos et al.

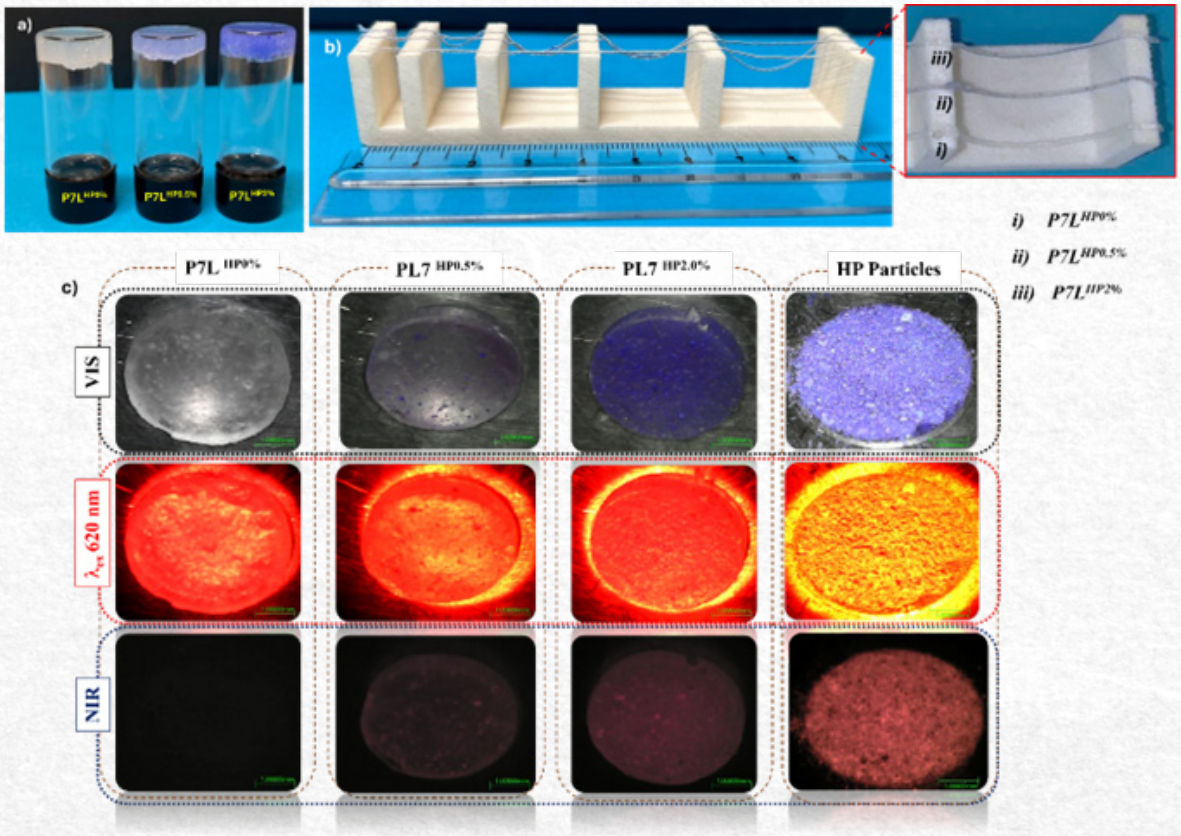

Figure 10 - (a) The sol-gel transition of gels over time through inversion test (after 24 hr); (b) Filament collapse testing and (c) Images of the samples at visible light (VIS), under excitation with red light (lex 620 nm), and the fluorescence NIR image (NIR). Source: Santos et al.

In the initial assessment, a manual extrusion pre-test of the gel filaments was carried out, depicted in Figure 10(b). This basic test aimed to evaluate how well the material can be printed and how filaments are formed [26,27]. After pushing the gels onto a surface, uninterrupted rods were created. Nevertheless, a significant deflection of the rods was observed due to the weight of the material, its viscosity, rheological characteristics, gravity's influence, and manual extrusion force. Despite this pronounced deflection, particularly over distances around 2.5 cm, no filament rupture occurred, ensuring that the material exhibited adequate elasticity and stability for subsequent gel printing.

In Figure 10(c), discs were molded from the gels to evaluate their luminescent properties. The samples were excited with monochromatic light at a central wavelength of 620 nm, close to the reported excitation maximum for HP[3]. The P7L$^{HP0.5\%}$ and P7L$^{HP2\%}$ gels exhibited fluorescence, attributed exclusively to the presence of the HP pigment, as illustrated in the image. Furthermore, the intensity of the NIR light emitted increased proportionally with the HP concentration in the discs. In contrast, the dark-field image reveals that the disc without HP (P7L$^{HP0\%}$) did not exhibit NIR fluorescence, demonstrating that the base gel alone lacks photoluminescent properties, which are entirely dependent on the presence of HP [2,28].

Following the preliminary tests conducted with the gels, the extrusion-printed scaffolds are presented in Figure 11. During the printing process, the samples containing 2% HP particles encountered significant challenges compared to the gels with 0.5% HP. These difficulties can be attributed to the high particle concentration and irregular morphology, which resulted in flow issues during printing. The irregularity of the particles led to the formation of aggregates, hindering the flow of the gel through the 410 µm diameter syringe nozzle, complicating the extrusion of gels with higher pigment concentration. However, this issue could be mitigated by using nozzles with larger diameters. Despite these challenges, as illustrated in Figure 11, the printed scaffolds exhibited good shape fidelity, with Pr values of 0.92 ± 0.06, 0.87 ± 0.01, and 0.89 ± 0.03 for the P7L$^{HP0\%}$, P7L$^{HP0.5\%}$, and P7L$^{HP2\%}$ gels, respectively. These findings suggest that the scaffolds closely resemble the intended design [26,27].

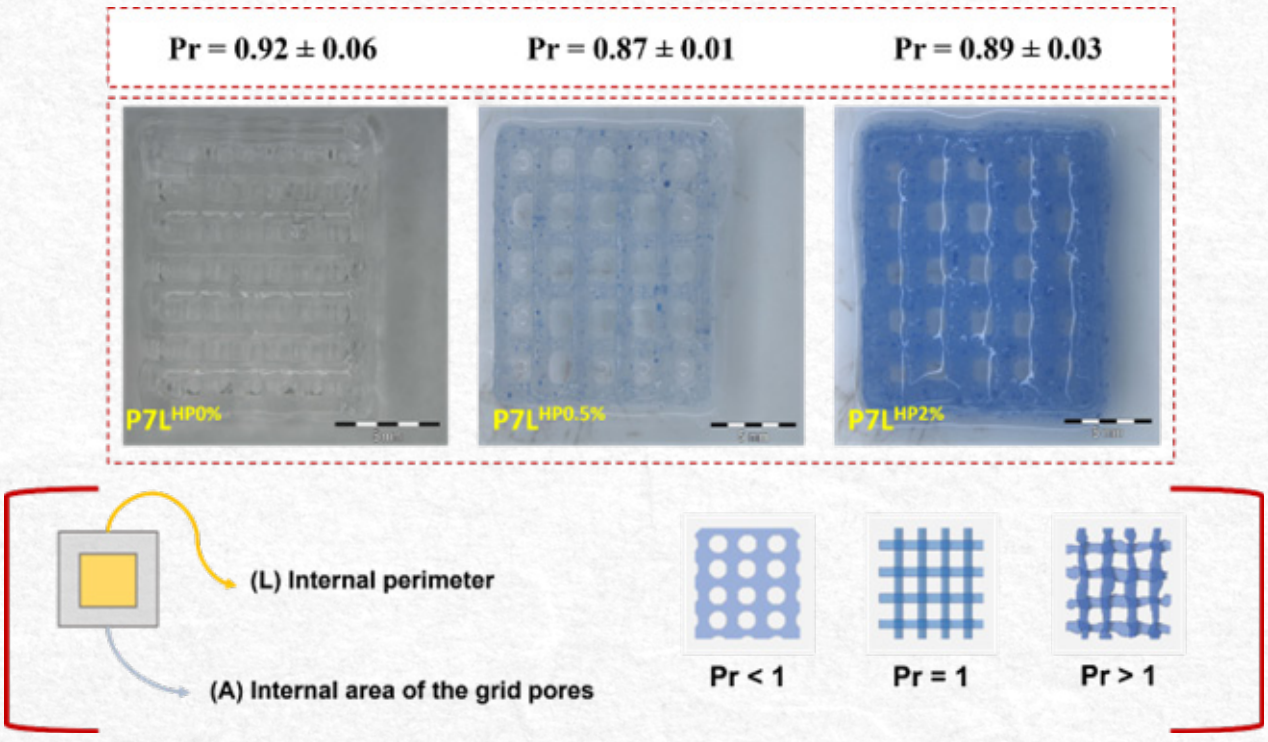

Figure 11 - Scaffolds obtained after printing gels containing HP at levels of 0.5% and 2% in their composition. Source: Santos et al.

Excitation and Emission Spectroscopy – Map of Printed Gels

As demonstrated in Figures 8 and 10, the dispersion of HP pigment was more efficient at the 2% concentration. For this reason, the intensity map of the scaffold was analyzed for this gel, as shown in Figure 12.

The excitation and emission map of the P7L$^{HP2\%}$ sample displays a maximum emission photoluminescence at 925 nm and maximum excitation at 625 nm, which are values consistent with those reported in the literature[2,21]. This is likely due to the energy levels of copper (Cu^{2+}), with the transitions selected for this optical thermometry analysis, indicating a potential application of this material in optical thermometry. However, it was also observed that the fluorescence of the material could be affected by the lack of particle treatment, as is typically performed with Egyptian Blue (EB), a pigment like HP [4].

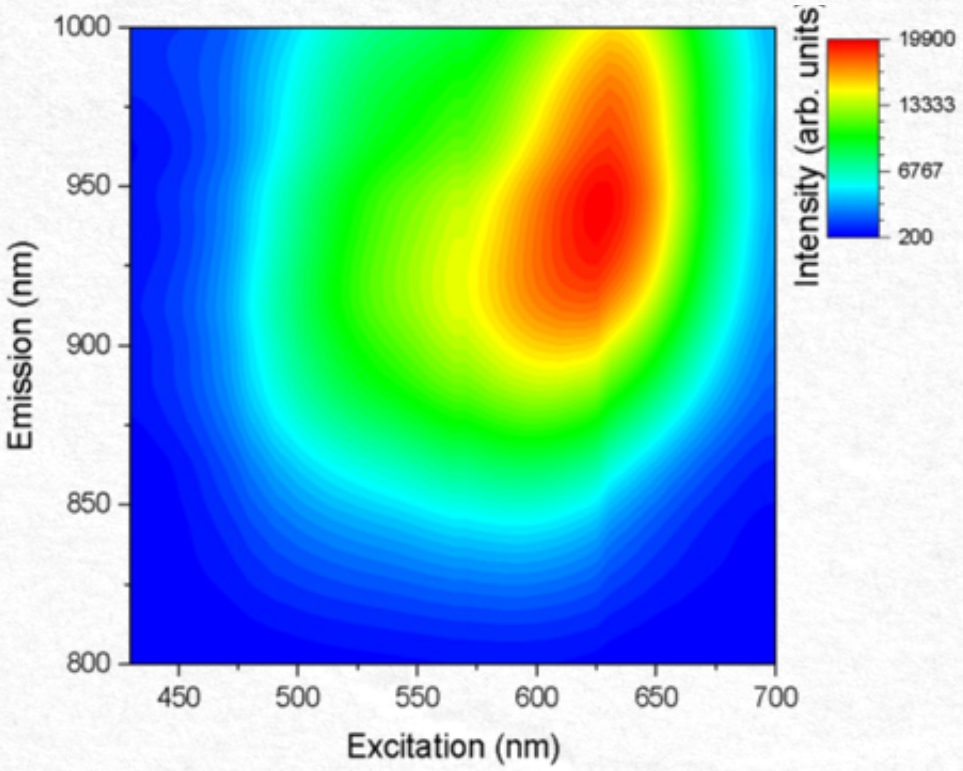

Figure 12 - Excitation versus emission map of the Scaffold produced with the P7LHP2% gel. Source: Santos et al.

Conclusion

In this study, we synthesized the HP pigment and explored its application in PEG-Laponite-based gels with concentrations of 0.5% and 2%. The resulting formulations exhibited luminescent properties and demonstrated good feasibility for constructing three-dimensional structures. Characterization of the synthesized compound confirmed the successful production of HP, which appeared as elongated particles with heterogeneous distribution. Furthermore, the incorporation of HP at the tested concentrations resulted in adequate dispersion within the gel network, as evidenced by photographic images. FTIR analysis verified the interactions between the PEG-Laponite phases and HP, identifying both physical interactions and the formation of new functional groups. Even when dispersed in the polymer matrix, HP retained its fluorescent properties, albeit with reduced intensity. In addition, the formulations exhibited favorable extrusion characteristics during 3D printing, culminating in the successful fabrication of scaffolds with high shape fidelity. These findings indicate that the use of HP as a dispersed phase in polymeric gels offers a promising innovation, with potential applications in biotechnology, such as in temperature sensors, near-infrared (NIR) imaging, and photothermal applications.

Acknowledgments

This paper is dedicated to the memory of Dr. Jorge V. Lopes da Silva. Sadly, he passed away before the submission of this study. We want to recognize not only his contribution to the conceptualization of this interesting line of research, but also his unconditional support for all of us during our careers as researchers.

We are grateful to Igor Leandro de Oliveira (CTI Renato Archer) for the mechanical technical support in the temperature-dependent emission experiments.

The authors would like to thank FINEP for

funding the EMUTISAÚDE project (grant no. 01.18.0027.00), and the CNPq/PCI program (process nos. 301583/2023-4, 300038/2024-0, and 300933/2024-0) for the financial support. This work was also supported by the National Council for Scientific and Technological Development (CNPq) (grant nos. 312216/2017-3 and 407680/2021-7), and the São Paulo Research Foundation (FAPESP) (process no. 2019/11950-6).

References

[1]. Bhatia SK, Bhatia S, Inda-Webb ME, Kourmentza K, Moon TS, Singh V, et al. Biotechnology for sustainable materials: innovating today for a greener tomorrow. Biotechnology for Sustainable Materials 2024;1(1).

[2]. Chen Y, Zhang Y, Feng S. Hydrothermal synthesis and properties of pigments Chinese purple $BaCuSi_2O_6$ and dark blue BaCu2Si 2O7. Dyes and Pigments 2014;105:167–73.

[3]. Pozza G, Ajò D, Chiari G, De Zuane F, Favaro M. Photoluminescence of the inorganic pigments Egyptian blue, Han blue and Han purple. J Cult Herit 2000;1(4):393–8.

[4]. Johnson-McDaniel D, Salguero TT. Exfoliation of Egyptian blue and han blue, two Alkali earth copper silicate-based pigments. Journal of Visualized Experiments 2014;(86):1–10.

[5]. Johnson-Mcdaniel D, Barrett CA, Sharafi A, Salguero TT. Nanoscience of an ancient pigment. J Am Chem Soc 2013;135(5):1677–9.

[6].. Iguchi M, Hiraga Y, Kasuya K, Aida TM, Watanabe M, Sato Y, et al. Viscosity and density of poly(ethylene glycol) and its solution with carbon dioxide at 353.2K and 373.2K at pressures up to 15MPa. J Supercrit Fluids [Internet] 2015; 97:63–73. Available from: https: //www.sciencedirect.com/science/article/pii/S0896844614003490

[7]. Daguano JKMB, Giora FC, Santos KF, Pereira ABGC, Souza MT, Dávila JL, et al. Shear-thinning sacrificial ink for fabrication of Biosilicate® osteoconductive scaffolds by material extrusion 3D printing. Mater Chem Phys 2022;287.

[8]. Davern JW, Hipwood L, Bray LJ, Meinert C, Klein TJ. Addition of Laponite to gelatin methacryloyl bioinks improves the rheological properties and printability to create mechanically tailorable cell culture matrices. APL Bioeng 2024;8(1).

[9]. Santos KF, Dávila JL, D'ávila MA, Rodas ACD, da Silva JVL, Daguano JKMB. Rheological study of PEG-Laponite-alginate composite hydrogels aiming 3D extrusion-based printing. Revista Materia 2022;27(2).

[10]. Brunchi CE, Morariu S. Laponite®—From Dispersion to Gel—Structure, Properties, and Applications. Molecules2024;29(12).

[11]. Dávila JL, Manzini BM, Lopes da Fonsêca JH, Mancilla Corzo IJ, Neto PI, Aparecida de Lima Montalvão S, et al. A parameterized g-code compiler for scaffolds 3D bioprinting. Bioprinting [Internet] 2022; 27: e 00222. Available from: https://www.sciencedirect.com/science/article/pii/S240588662200032X

[12]. Jongprasitkul H, Turunen S, Parihar VS, Kellomäki M. Two-step crosslinking to enhance the printability of methacrylated gellan gum biomaterial ink for extrusion-based 3D bioprinting. Bioprinting 2022;25.

[13]. Fu Z, Naghieh S, Xu C, Wang C, Sun W, Chen X. Printability in extrusion bioprinting. Biofabrication 2021;13(3).

[14]. Zhang Z, Ma Q, Berke H. Man-made blue and purple barium copper silicate pigments and the pabstite ($BaSnSi_3O_9$) mystery of ancient Chinese wall paintings from Luoyang. Herit Sci 2019;7(1).

[15]. Binet L, Lizion J, Bertaina S, Gourier D. Magnetic and New Optical Properties in the UV-visible Range of the Egyptian Blue Pigment Cuprorivaite CaCuSi4O10. Journal of Physical Chemistry C 2021;125(45):25189–96.

[16]. Wade SA, Collins SF, Baxter GW. Fluorescence intensity ratio technique for optical fiber point temperature sensing. J Appl Phys [Internet] 2003;94(8):4743–56. Available from: https://pubs.aip.org/jap/article/94/8/4743/471248/Fluorescence-intensity-ratio-technique-for-optical.

[17]. Morassuti CY, Nunes LAO, Lima SM, Andrade LHC. Eu^{3+} - doped alumino-phosphate glass for ratiometric thermometer based on the excited state absorption. J Lumin 2018;193(August 2017):39–43.

[18]. Morassuti CY, Finoto S, Silva JR, Lima SM, Andrade LH da C. A Novel Route for a Fluorescent Temperature Sensor Based on the Reabsorption Process in Sm^{2+}-Doped KCl. Phys Status Solidi B Basic Res 2020;257(8):1–6.

[19]. Lalla EA, León-Luis SF, Monteseguro V, Pérez-Rodríguez C, Cáceres JM, Lavín V, et al. Optical temperature sensor based on the Nd^{3+} infrared thermalized emissions in a fluorotellurite glass. J Lumin [Internet] 2015; 166:209–14. Available from: http://www.sciencedirect.com /science/article/pii/S0022231315002768

[20]. Morassuti CY, L Silva AP, Nunes LAO, Lima SM, Andrade LHC. Effect of radiative loss mechanisms on FIR thermometric parameters of Nd3+-doped lithium tellurite glasses. Journal of Rare Earths [Internet] 2023 Available from: https://linkinghub.elsevier.com/ retrieve/pii/S1002072123001539.

[21]. Smith AM, Mancini MC, Nie S. Second window for in vivo imaging. Nat Nanotechnol [Internet] 2009;4(11):710–1. Available from: http://dx.doi.org/10.1038/nnano.2009.326

[22]. Lin-Vien D, Colthup NB, Fateley WG, Grasselli JG (Professor). The Handbook of infrared and raman

characteristic frequencies of organic molecules. Academic Press 1991.

[23]. Fortunato G, Tatsi E, Corsini F, Turri S, Griffini G. Stimuli-Responsive Luminescent Solar Concentrators Based on Photoreversible Polymeric Systems. ACS Appl Polym Mater 2020;2(9):3828–39.

[24]. Rafael D, Andrade F, Martinez-Trucharte F, Basas J, Seras-Franzoso J, Palau M, et al. Sterilization procedure for temperature-sensitive hydrogels loaded with silver nanoparticles for clinical applications. Nanomaterials 2019;9(3).

[25]. Dessì M, Borzacchiello A, Mohamed THA, Abdel--Fattah WI, Ambrosio L. Novel biomimetic thermosensitive β-tricalcium phosphate/chitosan-based hydrogels for bone tissue engineering. J Biomed Mater Res A 2013;101(10):2984–93.

[26]. Ren H, Liu Y, Zhang R, Zheng Y, Zhao T, Han J, et al. Near-infrared carbon quantum dots from PEG-based deep eutectic solvents for high-accuracy quantitative analysis of naphthenic acids in wastewater. J Environ Chem Eng 2023;11:109988.

[27]. Temirel M, Dabbagh SR, Tasoglu S. Shape Fidelity Evaluation of Alginate-Based Hydrogels through Extrusion-Based Bioprinting. J Funct Biomater 2022;13(4).

[28]. Naghieh S, Chen X. Printability–A key issue in extrusion-based bioprinting. J Pharm Anal 2021;11(5):564–79.